

Test-time Adaptive Hierarchical Co-enhanced Denoising Network for Reliable Multimodal Classification

Shu Shen[✉], Student Member, IEEE, C. L. Philip Chen[✉], Life Fellow, IEEE, and Tong Zhang[✉], Senior Member, IEEE

Abstract—Reliable learning on low-quality multimodal data is a widely concerning issue, especially in safety-critical applications. However, multimodal noise poses a major challenge in this domain and leads existing methods to suffer from two key limitations. First, they struggle to reliably remove heterogeneous data noise, hindering robust multimodal representation learning. Second, they exhibit limited adaptability and generalization when encountering previously unseen noise. To address these issues, we propose Test-time Adaptive Hierarchical Co-enhanced Denoising Network (TAHCD). On one hand, TAHCD introduces the Adaptive Stable Subspace Alignment and Sample-Adaptive Confidence Alignment to reliably remove heterogeneous noise. They account for noise at both global and instance levels and enable jointly removal of modality-specific and cross-modality noise, achieving robust learning. On the other hand, TAHCD introduces test-time cooperative enhancement, which adaptively updates the model in response to input noise in a label-free manner, improving adaptability and generalization. This is achieved by collaboratively enhancing the joint removal process of modality-specific and cross-modality noise across global and instance levels according to sample noise. Experiments on multiple benchmarks demonstrate that the proposed method achieves superior classification performance, robustness, and generalization compared with state-of-the-art reliable multimodal learning approaches.

Index Terms—Multimodal classification, heterogeneous noise, robustness, adaptability, generalization ability.

I. INTRODUCTION

HUMANS perceive and understand the world through multiple sensory channels, such as vision, hearing, and smell. Inspired by this capability, multimodal learning [1]–[4] has gained substantial attention in deep learning. With recent advances in sensing, video technologies, and data processing, large volumes of multimodal data have become available, further accelerating progress in this field. By effectively fusing complementary information across modalities, multimodal learning enables more comprehensive and discriminative representations. As a result, it significantly improves performance across a wide range of tasks, including disease diagnosis [5], [6], image–text classification [7]–[9], video classification [10]–[12], and emotion analysis [13]–[15].

While multiple modalities enrich representation learning, they inevitably introduce more complex noise, typically arising from sensor errors, environmental interference, and data collection errors. In real-world scenarios, multimodal noise exhibits two key characteristics: (1) **Heterogeneity**. Previous work [16] identifies two main types of multimodal noise:

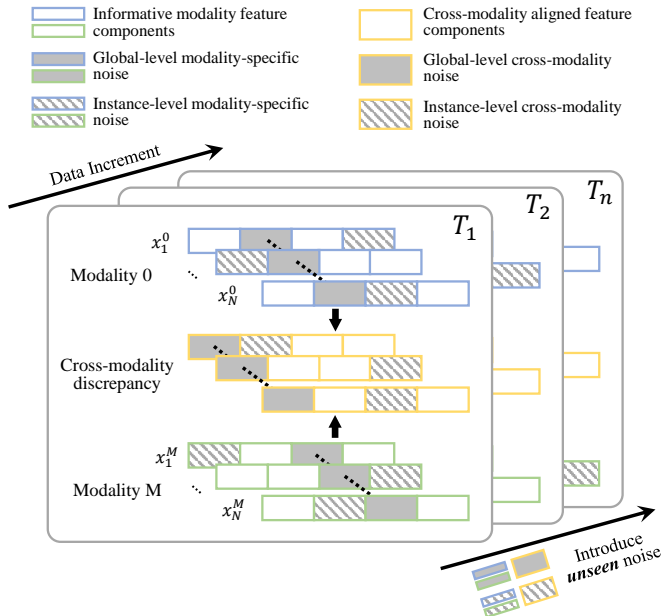


Fig. 1. Illustration of complex multimodal noise in real-world scenario. (i) **Heterogeneity**. Multimodal noise generally falls into two types [16]: modality-specific and cross-modality noise, which may occur at the global level across all samples or at the instance level in individual samples. (ii) **Unpredictability**. With incremental data acquisition, the noise evolves over time and may include previously unseen patterns.

modality-specific noise and **cross-modality noise**. Modality-specific noise arises independently in each modality from sensor errors or environmental disturbances, while cross-modality noise stems from low-quality data due to weakly aligned or misaligned multimodal samples [17], [18]. (2) **Unpredictability**. Noise often evolves over time as new samples are incrementally acquired, potentially introducing previously unseen noise. For example, in the medical domain, unexpected device failures may generate unfamiliar noise in newly collected patient data. In autonomous driving, sensors often face varying weather and urban conditions. In Internet data collection, diverse image–text–mismatched posts continuously emerge over time.

In the presence of complex multimodal noise, conventional multimodal methods struggle to produce reliable results, making them unsuitable for safety-critical applications such as computer-aided disease diagnosis and autonomous driving [19]–[21]. Accordingly, many methods improve the reliability

of multimodal learning by removing noise and uninformative feature in data. Among them, [5]–[8], [21]–[24] address modality-specific noise via confidence-based feature learning and fusion. However, they generally assume well-aligned inputs and overlook the presence of cross-modality noise. Conversely, [25]–[29] eliminate cross-modality noise via alignment and rectification, but their lack of modality-confidence awareness leads to limited robustness under modality-specific noise. Therefore, these methods generally face the following limitations. **(1) Insufficient robustness to heterogeneous noise:** They struggle to achieve joint removal of modality-specific and cross-modality noise. **(2) Limited generalization:** they can only learn and update on limited training data, making it difficult to handle previously unseen noise.

To address these limitations, we propose Test-time Adaptive Hierarchical Co-enhanced Denoising Network (TAHCD). TAHCD first removes heterogeneous noise by considering it at both global and instance levels. As shown in Fig. 1, data often contain global-level noise with consistent patterns across samples, such as persistent sensor faults or repeated sampling under identical conditions, and instance-level noise affecting individual samples, e.g., sudden sensor failures or human errors. Accordingly, TAHCD proposes Adaptive Stable Subspace Alignment (ASSA) and Sample-Adaptive Confidence Alignment (SACA) to jointly eliminate modality-specific and cross-modality noise at the global and instance levels, respectively, achieving robust representation learning. Moreover, TAHCD incorporates test-time cooperative enhancement (TTCE) to collaboratively refine global- and instance-level denoising based on input noise in a label-free manner, enabling adaptation to previously unseen noise and substantially improving generalization.

Specifically, ASSA first computes each modality's feature covariance and performs singular value decomposition. A learnable mask conditioned on the singular values then selects eigenvectors to construct stable feature subspaces, guided by inter-class orthogonality and subspace projection alignment. These constraints encourage the mask to discard directions carrying modality-specific and cross-modality noise across all samples. By aligning modality projections in the constructed stable subspaces, the subspace projection alignment in ASSA improves the reliability of cross-modality noise removal by preventing the model from erroneously aligning uninformative semantic content induced by modality-specific noise. Subsequently, SACA uses the globally denoised features from ASSA to estimate priors that guide the experts in removing heterogeneous noise at the instance level via a confidence-aware asymmetric slack alignment. By reweighting gradients based on modality confidence, this strategy encourages low-confidence modalities to align towards high-confidence ones, enabling reliable cross-modality noise removal under instance-level modality-specific noise. It also adopts a slack alignment scheme that constrains cross-modality discrepancies within a reasonable range learned from the prior, reflecting inherent differences in informative content across modalities. Compared with existing methods that strictly enforce cross-modality consistency, this prevents over-suppressing modality-specific complementary information while removing noise, resulting

in more robust multimodal representations.

Building upon the above framework for heterogeneous noise removal, we further propose TTCE that adapts the denoising framework to unseen noise in a label-free manner. Since the instance level can capture noise variations more sensitively than the global level, it can also perceive unseen noise more accurately. Based on this consideration, TTCE first incorporates the instance-level modality-specific and cross-modality noise learned by SACA into the reconstruction of globally denoised modality features produced by ASSA. This enables global-level modality representation learning in ASSA to explicitly leverage more accurate and finer-grained unseen-noise information captured at the instance level, thereby improving global-level unseen-noise removal. The enhanced global-denoised features in ASSA can provide more reliable priors, which in turn improve instance-level unseen-noise learning and removal in SACA. Through multiple iterations of the above ASSA–SACA co-enhancement process, the model achieves progressive update and adaptation to unseen noise.

The contributions of this paper can be summarized as:

- We propose TAHCD, which jointly removes modality-specific and cross-modality noise across global and instance levels via ASSA and SACA while adapting to previously unseen noise. It achieves SOTA results across multiple benchmarks under diverse noise conditions.
- ASSA's subspace projection alignment and SACA's confidence-aware asymmetric slack alignment mitigate modality-specific noise interference and preserve complementary modality feature during cross-modality noise removal, facilitating joint removal of both noise types.
- The proposed TTCE in TAHCD cooperatively enhances ASSA and SACA driven by input sample noise in a label-free manner. This enables adaptive improvement of the denoising process at test time for previously unseen noise, thereby enhancing model generalization ability.

II. RELATED WORKS

This section briefly reviews related works on multimodal learning and reliable learning from noisy, low-quality multimodal data.

A. Multimodal Learning

The advancement of sensor technology and the development of data transmission methods have led to the emergence of a vast amount of data from diverse sources, types, and formats. This has driven the rapid growth of multimodal learning [4], [30], [31], which has substantially improved machine learning performance across a wide range of tasks and applications [32]–[34]. For instance, in biomedical applications, DeepIMV [35] and MOGONET [36] have achieved more precise pathological classification by integrating multiple omics data. In computer vision, CEN [37] has enhanced dense image prediction by fusing multimodal data and adaptively exchanging channels of different modality models. Zhang et al. [2] have guided image outpainting more effectively by balancing the fusion of image and text modalities. In recent years, growing attention has been directed toward addressing

the challenges of multimodal learning in real-world scenarios, one of which is the need to handle low-quality multimodal data. [7], [16]. However, conventional multimodal learning methods struggle to produce robust and generalizable outputs when faced with low-quality data, making it difficult to meet the reliability requirements of the model, especially in safety-critical applications. Consequently, we propose a method for reliable multimodal learning that learns robust representations under heterogeneous noise while effectively adapting and generalizing under unseen noise.

B. Reliable Learning from Low-Quality Multimodal Data

In real-world scenarios, multimodal learning often suffers from low-quality data, which undermines reliability. A major source of such low-quality data is multimodal noise, typically arising from factors such as sensor failures, environmental influences, or human errors. Existing studies [16] categorize multimodal noise into two types, namely modality-specific noise and cross-modality noise, and have developed various methods to address these noise types for reliable multimodal learning.

Many studies mitigate noise in each modality and improved robustness through confidence-based representation learning and fusion methods. For instance, Federici et al. [38] have proposed the multi-view information bottleneck, which has improved the robustness of multi-view learning by retaining information shared by each view. Han et al. [22] have parameterized the evidence of different modality features using Dirichlet distribution and fused each modality at the evidence level using Dempster-Shafer theory. Geng et al. [24] have proposed the DUA-Nets, which achieved uncertainty-based multimodal representation learning through reconstruction. Han et al. [5] have modeled informativeness at the feature and modality levels, achieving trustworthy multimodal feature fusion. Zhang et al. [7] have achieved more robust multimodal fusion by dynamically assigning weights to each modality based on uncertainty estimation. Zheng et al. [39] have achieved trustworthy multimodal classification via integrating feature and label-level confidence. Zou et al. [6] have proposed a novel dynamic poly-attention Network that integrated global structural information for trustworthy multimodal classification. Zhou et al. [21] have introduced a trustworthy multi-view classification framework by enhancing multi-view encoding and confidence-aware fusion. Cao et al. [8] have proposed the Predictive Dynamic Fusion method, which provides theoretical guarantees for reducing the upper bound of generalization error in dynamic multimodal fusion.

Additionally, many studies focus on cross-modality noise removal by modeling alignment and correspondence between modalities. Radenovic et al. [40], Gadre et al. [41], and Sharma et al. [42] have proposed rule-based methods to remove misaligned or weakly aligned data. NCR [43], ALBEF [44], BLIP [45], and SPS [29] have adopted model-based rectification methods, which design models to filter or correct misaligned samples. Additionally, NLIP [25], OSCAR [26], and SMILE [28] have proposed noise-robust regularization methods to mitigate the impact of misaligned samples on the model.

Although the aforementioned methods effectively remove multimodal noise and enhance the reliability of representation learning, they generally exhibit the following limitations. First, they struggle to jointly remove modality-specific and cross-modality noise, resulting in representations with limited robustness under heterogeneous data noise. Moreover, they can only learn and update on limited training data, making them poorly adaptive to unseen noise and limiting generalization. To address these issues, we propose Test-time Adaptive Hierarchical Co-enhanced Denoising Network (TAHCD), which jointly removes modality-specific and cross-modality noise at both global and instance levels, and enables label-free, adaptive updates to model inputs at test time, significantly improving robustness and generalization.

III. PROPOSED APPROACH

In this section, we provide a detailed introduction of the proposed Test-time Adaptive Hierarchical Co-enhanced Denoising Network (TAHCD). Let $\mathcal{D} = \{(x_i, y_i)\}_{i=1}^N$ denote a multimodal dataset with N samples, where each sample contains M modalities and is assigned one of C class labels. The objective of multimodal classification is to train a neural network that maps each input $x_i = \{x_i^m \in \mathbb{R}^{d^m}\}_{m=1}^M$ to its corresponding label $y_i \in \mathbb{R}^C$, with d^m representing the feature dimension of the m -th modality. However, dataset \mathcal{D} typically contains complex multimodal noise, which undermines the reliability of multimodal classification. To this end, we propose TAHCD, which jointly removes modality-specific and cross-modality noise at global and instance levels and adaptively updates to input noise in a label-free manner, enabling robust and generalizable multimodal classification.

A. Overview of TAHCD

As illustrated in Fig. 2, TAHCD first employs modality-specific feature encoders to extract representations from each modality. It then introduces Adaptive Stable Subspace Alignment (ASSA) to remove modality-specific and cross-modality noise exhibiting global distributional characteristics. In addition, Sample-Adaptive Confidence Alignment (SACA) is proposed to eliminate modality-specific and cross-modality noise at the instance level. Building upon these components, we further design test-time cooperative enhancement (TTCE) mechanism. It achieves cooperative enhancement between global- and instance-level denoising, driven by sample noise in a label-free manner, improving adaptability and generalization to unseen noise.

B. Adaptive Stable Subspace Alignment

To eliminate modality-specific noise and cross-modality noise with global characteristics across all samples in multimodal features, the Adaptive Stable Subspace Alignment (ASSA) strategy is proposed. ASSA adaptively selects highly informative principal axes in the feature space to construct a stable feature subspace. Subsequently, inter-class orthogonality constraints within each modality are imposed to ensure that the learned subspaces effectively suppress modality-specific noise.

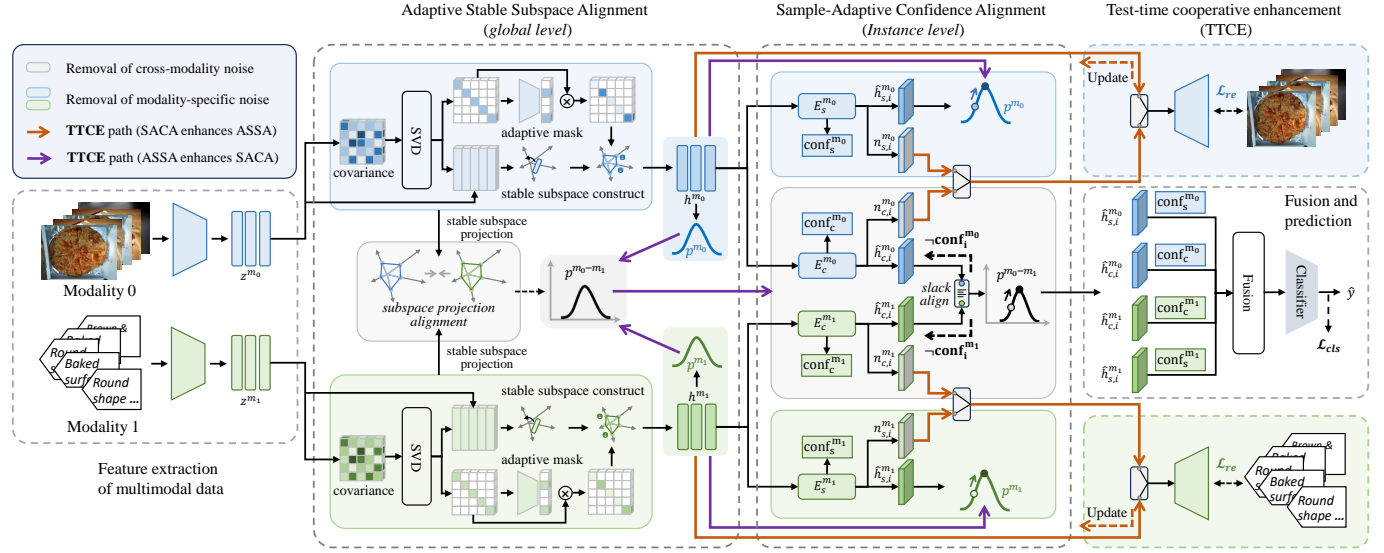


Fig. 2. The framework diagram of the Test-time Adaptive Hierarchical Co-enhanced Denoising Network (TAHCD), best viewed in color. TAHCD consists of three key components: (1) Adaptive Stable Subspace Alignment (ASSA): jointly removes modality-specific and cross-modality noise at the global level. (2) Sample-Adaptive Confidence Alignment (SACA): jointly removes modality-specific and cross-modality noise at the instance level. (3) Test-Time Cooperative Enhancement (TTCE): adaptively enhances the model in response to test-time noise. Without loss of generality, the diagram illustrates a scenario with two modalities, where the blue and green colors represent two distinct modalities.

Furthermore, we introduce a subspace projection alignment constraint to prevent erroneous alignment of uninformative semantic content under modality-specific noise and enhance cross-modality noise removal.

1) *Adaptive Stable Subspace Construction*: To facilitate global-level multimodal noise removal, we adaptively eliminate statistically unstable and uninformative directions in the feature distribution of each modality and suppress noise-dominated variations across samples. Specifically, for the m -th modality, the input $x^m = \{x_1^m, \dots, x_N^m\}$ is first encoded into the latent space $z^m = \{z_1^m, \dots, z_N^m\}$ by the corresponding modality encoder ϕ_x^m : $z^m = \phi_x^m(x^m)$. Then, the covariance matrix Σ_z^m among features is computed from z^m , which can be formulated as follows:

$$\Sigma_z^m = \mathbb{E} [(z^m - \mu_z^m)(z^m - \mu_z^m)^\top] \in \mathbb{R}^{d^m \times d^m}, \quad (1)$$

where

$$\mu_z^m = \frac{1}{N} \sum_{i=1}^N z_i^m \in \mathbb{R}^{d_m}. \quad (2)$$

Subsequently, we perform singular value decomposition on the covariance matrix Σ_z^m , which can be expressed as:

$$\Sigma_z^m = U_z^m \Lambda_z^m (U_z^m)^\top. \quad (3)$$

$U_z^m = [u_1^m, \dots, u_{d^m}^m]$ is the matrix of orthogonal eigenvectors, and $\Lambda_z^m = \text{diag}(\lambda_1^m, \dots, \lambda_{d^m}^m)$ contains the non-negative singular values. Each vector u_i^m ($i \in [1, d^m]$) in U_z^m represents a principal axis in the feature space, while the corresponding singular value λ_i^m denotes the variance along that axis and is closely related to its informativeness. Therefore, we propose to learn a mask w_λ^m from the singular values $\lambda^m = [\lambda_1^m, \dots, \lambda_{d^m}^m]$ to adaptively select informative principal axes while suppressing noisy and redundant ones,

thereby achieving global-level noise removal on z^m . This process can be formulated as:

$$w_\lambda^m = \sigma(\phi_\lambda^m(\lambda^m)) \in \mathbb{R}^{d^m}, \quad (4)$$

$$h^m = z^m U_z^m \text{diag}(w_\lambda^m) (U_z^m)^\top. \quad (5)$$

$\phi_\lambda^m(\cdot)$ is a learnable encoder, $\sigma(\cdot)$ denotes the sigmoid function. $h^m = \{h_1^m, \dots, h_N^m\}$ denote the globally denoised representation obtained from the latent feature z^m of modality m . As shown in Eq. (5), the feature vector z^m is first projected onto the covariance principal axes using the orthogonal basis U_z^m . It is then filtered by the learned mask w_λ^m and finally mapped back to the original feature space via $(U_z^m)^\top$.

2) *Constraints*: To ensure that the adaptive stable subspace construction sufficiently eliminates modality-specific and cross-modality noise, we introduce inter-class orthogonality constraint \mathcal{L}_o and subspace projection alignment constraint \mathcal{L}_a . The inter-class orthogonality constraint \mathcal{L}_o eliminates modality-specific noise by removing the shared spurious patterns it induces across classes within the same modality, while preserving class-discriminative features, which can be formulated as:

$$\mathcal{L}_o = \frac{1}{C(C-1)} \sum_{m=1}^M \sum_{c=1}^C \sum_{c' \neq c}^C \|(\mu^{m,c})^\top \cdot \mu^{m,c'} - I\|_F^2. \quad (6)$$

$\mu^{m,c} = \frac{1}{|x^{m,c}|} \sum_{i=1}^{|x^{m,c}|} x_i^{m,c}$, where $x^{m,c} = \{x_i^{m,c}\}_{i=1}^{|x^{m,c}|}$ denotes the set of modality- m features for all samples belonging to class c , and $|\cdot|$ represents the cardinality of the set. $I \in \mathbb{R}^{C \times C}$ denotes the identity matrix.

Additionally, the subspace projection alignment constraint \mathcal{L}_a removes cross-modality noise by aligning the projections of representations from different modalities within their respective stable subspaces, as shown in Eq. (7). By projecting modality features into their respective stable subspaces before

alignment, it mitigates the impact of noise in each modality on alignment learning, ensuring stable and reliable cross-modality correspondences.

$$\mathcal{L}_a = \sum_{m=1}^M \sum_{m' \neq m}^M \|z^m U_z^m \text{diag}(w_\lambda^m) - z^{m'} U_z^{m'} \text{diag}(w_\lambda^{m'})\|_F^2. \quad (7)$$

Based on the above constraints, we minimize the total loss $\mathcal{L}_{\text{assa}}$ defined in Eq. (8) to remove global-level noise in ASSA.

$$\mathcal{L}_{\text{assa}} = \mathcal{L}_o + \mathcal{L}_a. \quad (8)$$

C. Sample-Adaptive Confidence Alignment

To provide reliable supervision signals for instance-level noise removal, we first estimate modality-wise feature distributions and cross-modality discrepancy distributions using the globally denoised representations obtained from ASSA. These distributions are then serve as priors to guide sample-adaptive modality-specific and cross-modality noise experts with confidence-aware asymmetric slack alignment for instance-level noise removal.

1) *Prior Estimation*: Based on the representations $\{h^m\}_{m=1}^M$ of different modalities obtained from Eq. (5) in ASSA, we estimate the modality-wise feature distributions $\{h^m \sim p_h^m = \mathcal{N}(\mu_h^m, \Sigma_h^m)\}_{m=1}^M$ and cross-modality discrepancy distributions $\{(h^m - h^{m'}) \sim p_h^{m-m'} = \mathcal{N}(\mu_h^{m-m'}, \Sigma_h^{m-m'})\}_{m' \neq m}^M$. Specifically, for the modality-wise feature distribution p_h^m , we use maximum likelihood estimation to calculate μ_h^m and Σ_h^m from h^m , which can be obtained by replacing z^m in Eq. (2) and Eq. (1) with h^m , respectively. Subsequently, we compute the distribution of $(h^m - h^{m'})$ between any two distinct modalities m and m' as the cross-modality discrepancy distribution $p_h^{m-m'}$, whose mean $\mu_h^{m-m'}$ and covariance $\Sigma_h^{m-m'}$ can be obtained by:

$$\begin{aligned} \mu_h^{m-m'} &= \mu_h^m - \mu_h^{m'} \\ \Sigma_h^{m-m'} &= \Sigma_h^m + \Sigma_h^{m'} \end{aligned} \quad (9)$$

2) *Sample-Adaptive Noise Expert*: Modality-specific and cross-modality noise experts are then introduced to perform noise removal on each sample under the guidance of the estimated priors. Specifically, we introduce M modality-specific noise experts E_s^1, \dots, E_s^M and M cross-modality noise experts E_c^1, \dots, E_c^M , each corresponding to one modality. For a multimodal sample $x_i = \{x_i^m\}_{m=1}^M$ with globally denoised representation $h_i = \{h_i^m\}_{m=1}^M$, each modality representation h_i^m is fed into E_s^m and E_c^m to learn masks $w_{s,i}^m$ and $w_{c,i}^m$ that capture feature-wise informativeness relevant to modality-specific and cross-modality noise, respectively. These masks are then used to remove the modality-specific and cross-modality noise components $n_{s,i}^m, n_{c,i}^m$ from h_i^m and yield the corresponding denoised features $\hat{h}_{s,i}^m, \hat{h}_{c,i}^m$. The calculation in E_s^m can be formulated as:

$$\begin{aligned} w_{s,i}^m &= \sigma(\phi_s^m(h_i^m)) \in \mathbb{R}^{d^m}, \\ \hat{h}_{s,i}^m &= h_i^m \odot w_{s,i}^m, \quad n_{s,i}^m = h_i^m \odot (1 - w_{s,i}^m). \end{aligned} \quad (10)$$

The calculation in E_c^m can be formulated as:

$$\begin{aligned} w_{c,i}^m &= \sigma(\phi_c^m(h_i^m)) \in \mathbb{R}^{d^m}, \\ \hat{h}_{c,i}^m &= h_i^m \odot w_{c,i}^m, \quad n_{c,i}^m = h_i^m \odot (1 - w_{c,i}^m). \end{aligned} \quad (11)$$

ϕ_s^m and ϕ_c^m denote the learnable networks in E_s^m and E_c^m , respectively, and σ represents the sigmoid function. The operator \odot denotes element-wise multiplication.

3) *Confidence-Aware Asymmetric Slack Alignment*: We minimize the negative log-likelihood $\mathcal{L}_{\text{nll}}^s$ for $\hat{h}_s^m = \{\hat{h}_{s,i}^m\}_{i=1}^N$ under p_h^m , and $\mathcal{L}_{\text{nll}}^c$ for the cross-modality discrepancy $\hat{h}_c^{m-m'} = \{\hat{h}_{c,i}^m - \hat{h}_{c,i}^{m'}\}_{i=1}^N$ under the cross-modality discrepancy distribution $p_h^{m-m'}$, to respectively ensure effective removal of modality-specific and cross-modality noise in each sample. The overall objective $\mathcal{L}_{\text{saca}}$ is formulated as:

$$\begin{aligned} \mathcal{L}_{\text{saca}} &= \mathcal{L}_{\text{nll}}^s + \mathcal{L}_{\text{nll}}^c \\ &= - \sum_{m=1}^M \log p_h^m(\hat{h}_s^m) - \sum_{m=1}^M \sum_{m' > m}^M \log p_h^{m-m'}(\hat{h}_c^m - \hat{h}_c^{m'}). \end{aligned} \quad (12)$$

It is worth noting that, in $\mathcal{L}_{\text{nll}}^c$, unlike existing methods that remove cross-modality noise by maximizing inter-modality feature similarity, we instead constrain the feature discrepancies across modalities within a reasonable range. This range accounts for the inherent informative information differences across modalities, which is learned by the cross-modality discrepancy distribution $p_h^{m-m'}$. We refer to this strategy as **slack alignment**, which enables the removal of cross-modality noise while preserving more modality-specific complementary information, thereby facilitating more reliable multimodal representation learning. Moreover, considering confidence differences across modalities under modality-specific noise, we implement the slack alignment in an **asymmetric manner directed by modality confidence**. This encourages low-confidence modality features to align toward high-confidence ones, imposing stronger rectification on them, instead of rectifying uniformly across all modalities. Specifically, the update of the parameters in cross-modality noise expert E_c^m under the guidance of modality confidence can be expressed as:

$$\theta_c^m \leftarrow \theta_c^m - \eta \cdot \frac{1}{|B|} \sum_i^{|B|} \negconf_i^m \cdot \nabla_{\theta_c^m} \mathcal{L}_{\text{nll}}^c(\hat{h}_c^m; \theta_c^m). \quad (13)$$

θ_c^m denotes the network parameters of the cross-modality noise expert E_c^m , η is the learning rate, B is a random mini-batch, and $\nabla_{\theta_c^m} \mathcal{L}_{\text{nll}}^c$ represents the gradient of θ_c^m with respect to $\mathcal{L}_{\text{nll}}^c$. \negconf_i^m is a factor negatively correlated with the confidence of modality m feature h_i^m and can be dynamically computed during training as follows:

$$\negconf_i^m = \frac{\exp(1 - \tanh(c_i^m))}{\sum_{m'=1}^M \exp(1 - \tanh(c_i^{m'}))}, \quad (14)$$

where $c_i^m = p^m(h_i^m)$ is the confidence of sample feature h_i^m of modality m , estimated as its likelihood under the modality- m feature prior p^m . In this way, we amplify the update gradients of cross-modality noise experts responsible for low-confidence modality representations while reducing those for high-confidence ones. This encourages the model to focus on mining and applying stronger alignment rectification to

low-confidence modalities with pronounced modality-specific noise, while applying weaker rectification to high-confidence ones with less modality-specific noise. Consequently, cross-modality noise is more effectively mitigated in the presence of modality-specific noise, promoting the joint removal of both noise types.

D. Test-Time Cooperative Enhancement

ASSA and SACA establish a framework for jointly removing modality-specific and cross-modality noise at both global and individual levels to achieve robust learning. Building upon this framework, we introduce Test-Time Cooperative Enhancement (TTCE), which performs adaptive model updates driven by sample noise in a label-free manner to enhance the model's generalization to unseen noise. Specifically, TTCE is designed as a cooperative enhancement mechanism between ASSA and SACA conditioned on unseen noise.

Considering that instance-level representations are more sensitive to noise variations than global distributions, TTCE first enhance global-level denoising of ASSA using the learned instance-level noise from SACA. Specifically, we incorporate instance-level modality-specific and cross-modality noise components $n_s^m = \{n_{s,i}^m\}_{i=1}^N$ and $n_c^m = \{n_{c,i}^m\}_{i=1}^N$ from SACA into the globally denoised modality features h^m from ASSA and define a reconstruction loss:

$$\mathcal{L}_{\text{re}} = \frac{1}{M} \sum_{m=1}^M \|\Psi^m(h^m + n_s^m + n_c^m) - x^m\|_{\text{F}}^2. \quad (15)$$

$\Psi^m(\cdot)$ denotes the decoder corresponding to modality m , and $\|\cdot\|_{\text{F}}^2$ denotes the Frobenius norm. Minimizing \mathcal{L}_{re} enables ASSA to explicitly account for more accurate and finer-grained unseen-noise information captured at the instance level, yielding more robust globally denoised modality representations $h^{m\uparrow}$ to unseen noise. The process of enhancing h^m to $h^{m\uparrow}$ via \mathcal{L}_{re} can be expressed as:

$$\begin{aligned} h^{m\uparrow} &= h^m - \eta \frac{\partial \mathcal{L}_{\text{re}}}{\partial h^{m\uparrow}} \\ &= h^m - 2\eta J_{\Psi^m}(I_t^m)^\top (\Psi^m(I_t^m) - x^m), \end{aligned} \quad (16)$$

where $h^{m\uparrow}$ is initialized as h^m at the beginning of the update process. $I_t^m = \tilde{z}_t^m + n_s^m + n_c^m$. J_{Ψ^m} represents the Jacobian matrix of the decoder Ψ^m evaluated at the input. η is the learning rate.

Moreover, the enhanced modality features $h^{m\uparrow}$ in ASSA can help remove unseen noise from the priors, which in turn facilitating instance-level denoising in SACA. Specifically, for the modality-wise distribution $p^m \sim \mathcal{N}(\mu^m, \Sigma^m)$, we compute $\Delta\mu^{m\uparrow}$ and $\Delta\Sigma^{m\uparrow}$ by substituting z^m with $h^{m\uparrow}$ in Eqs. (2) and (1), respectively, and use them to update μ^m and Σ^m :

$$\begin{aligned} \mu^{m\uparrow} &= \alpha \cdot \mu^m + (1 - \alpha) \cdot \Delta\mu^{m\uparrow}, \\ \Sigma^{m\uparrow} &= \beta \cdot \Sigma^m + (1 - \beta) \cdot \Delta\Sigma^{m\uparrow}. \end{aligned} \quad (17)$$

$\mu^{m\uparrow}$ and $\Sigma^{m\uparrow}$ are the mean and covariance of the updated modality-wise distribution p^m , denoted as $p^{m\uparrow}$. α and β are two hyperparameters. Accordingly, the cross-modality discrepancy distribution $p^{m-m'}(m, m' \in [1, M], m \neq m')$ is updated to $p^{m-m'\uparrow} \sim \mathcal{N}(\mu^{m-m'\uparrow}, \Sigma^{m-m'\uparrow})$, with $\mu^{m-m'\uparrow}$

Algorithm 1 Inference procedure of TAHCD with TTCE

Input: Multimodal input $X = \{\{x_i^m\}_{i=1}^N\}_{m=1}^M$, trained ASSA and SACA.

- 1: Compute h^m with ASSA by Eq. (5).
- 2: Estimate priors $p^m, p^{m-m'}$ by Eqs. (1), (2), and (9).
- 3: Compute $\hat{h}_s^m, \hat{h}_c^m, n_s^m, n_c^m$ in SACA by Eqs. (10), (11).
- 4: **for** $e = 1, \dots, E$ **do**
- 5: Calculate \mathcal{L}_{re} using Eq. (15).
- 6: Enhance ASSA and $h^{m\uparrow}$ using Eq. (16).
- 7: Update priors $p^{m\uparrow}, p^{m-m'\uparrow}$ using Eq. (17) and (9).
- 8: Enhance SACA and $\hat{h}_s^{m\uparrow}, \hat{h}_c^{m\uparrow}$ using Eq. (18).
- 9: **end for**
- 10: Fuse $\{\hat{h}_s^m\}_{m=1}^M, \{\hat{h}_c^m\}_{m=1}^M$ using Eq. (19) for prediction.

and $\Sigma^{m-m'\uparrow}$ derived from $\mu^{m\uparrow}, \mu^{m'\uparrow}, \Sigma^{m\uparrow}$, and $\Sigma^{m'\uparrow}$ through Eq. (9). The enhanced priors $p^{m\uparrow}, p^{m'\uparrow}$, and $p^{m-m'\uparrow}$ are then applied in $\mathcal{L}_{\text{saca}}$ defined in Eq. (12) to improve the instance-level noise removal of the noise experts against unseen noise, which can be formulated as:

$$\begin{aligned} \hat{h}_s^{m\uparrow} &= \hat{h}_s^{m\uparrow} - \eta \frac{\partial \mathcal{L}_{\text{saca}}}{\partial \hat{h}_s^{m\uparrow}} = \hat{h}_s^{m\uparrow} - \eta (\Sigma^{m\uparrow})^{-1} (\hat{h}_s^{m\uparrow} - \mu^{m\uparrow}), \\ \hat{h}_c^{m\uparrow} &= \hat{h}_c^{m\uparrow} - \eta \frac{\partial \mathcal{L}_{\text{saca}}}{\partial \hat{h}_c^{m\uparrow}} \\ &= \hat{h}_c^{m\uparrow} - \eta \sum_{m' \neq m}^M (\Sigma^{m-m'\uparrow})^{-1} (\hat{h}_c^{m\uparrow} - \hat{h}_c^{m'\uparrow} - \mu^{m-m'\uparrow}). \end{aligned} \quad (18)$$

Therefore, through multiple iterations of the above ASSA–SACA cooperative enhancement, TTCE progressively updates the model to adapt to unseen noise. For clarity, the overall inference procedure of TAHCD with TTCE is summarized in Algorithm 1, where E denotes the number of cooperative enhancement iteration between ASSA and SACA and is analyzed in Sec. IV-G.

E. Training and Inference

Finally, we fuse the multimodal features produced by sample-adaptive noise experts after TTCE, weighted by their respective confidence scores. Specifically, the confidence score is first estimated as the likelihood of the input feature vector under the corresponding modality-wise distribution: $\text{conf}_s^{m\uparrow} = p^{m\uparrow}(\hat{h}_s^{m\uparrow})$, $\text{conf}_c^{m\uparrow} = p^{m\uparrow}(\hat{h}_c^{m\uparrow})$. We then normalize the output confidences of all experts to obtain weights $\{\text{conf}_s^{m\uparrow}\}_{m=1}^M, \{\text{conf}_c^{m\uparrow}\}_{m=1}^M$, which are used to fuse $\{h_s^{m\uparrow}\}_{m=1}^M, \{h_c^{m\uparrow}\}_{m=1}^M$:

$$f^{mm} = \sum_{m=1}^M (\text{conf}_s^{m\uparrow} \cdot \hat{h}_s^{m\uparrow} + \text{conf}_c^{m\uparrow} \cdot \hat{h}_c^{m\uparrow}). \quad (19)$$

The obtained multimodal feature f^{mm} is fed into a classifier to produce the prediction \hat{y} , and the loss is computed using the cross-entropy with the ground-truth label: $\mathcal{L}_{\text{cls}} = \text{CE}(y, \hat{y})$, where $\text{CE}(\cdot)$ is the cross-entropy function. TAHCD is trained using the total loss $\mathcal{L}_{\text{tot}} = \mathcal{L}_{\text{assa}} + \mathcal{L}_{\text{saca}} + \mathcal{L}_{\text{re}} + \mathcal{L}_{\text{cls}}$, where the prediction is obtained from modality features after E iterations of enhancement in TTCE. $\mathcal{L}_{\text{assa}}$, $\mathcal{L}_{\text{saca}}$, and \mathcal{L}_{re} are defined in Eqs. (8), (12), and (15), respectively. The inference procedure during testing of TAHCD is shown in Algorithm 1.

TABLE I

COMPARISON OF CLASSIFICATION PERFORMANCE BETWEEN THE PROPOSED TAHCD AND OTHER RELIABLE MULTIMODAL CLASSIFICATION METHODS ON THE BRCA, ROSMAP, CUB, AND UPMC FOOD101 DATASETS, WHERE BOTH TRAINING AND TESTING ARE CONDUCTED UNDER THE SAME NOISE SETTINGS. THE BEST RESULTS UNDER VARIOUS NOISE SETTINGS ARE INDICATED IN **BOLD**, WHILE THE SECOND-BEST RESULTS ARE UNDERLINED.

Data Type	Methods	BRCA			ROSMAP			CUB			FOOD101		
		ACC	WeightedF1	MacroF1	ACC	F1	AUC	ACC	WeightedF1	MacroF1	ACC	WeightedF1	MacroF1
$\eta = 0$ $\epsilon = 0$	MD [5]	83.7	83.6	79.9	83.0	83.0	90.2	91.9	92.0	91.9	92.3	92.7	92.7
	MLCLNet [39]	82.3	82.2	78.6	79.4	79.2	89.3	90.2	90.3	89.9	92.1	92.2	92.1
	QMF [7]	82.5	82.3	79.1	78.3	78.1	85.1	88.3	88.3	87.9	91.7	92.2	92.1
	PDF [8]	82.1	81.7	76.4	80.2	82.9	87.1	89.2	89.1	88.9	92.2	92.4	92.3
	NCR [43]	77.9	75.3	71.1	79.2	80.0	87.4	83.9	83.7	84.0	91.1	91.5	91.5
	ALBEF [44]	78.2	75.2	71.3	79.0	80.3	86.5	84.0	84.2	84.2	91.2	91.5	91.4
	SMILE [28]	80.5	81.0	78.2	79.2	79.5	87.4	88.6	88.6	88.3	91.3	91.7	91.6
	SPS [29]	79.8	80.3	78.4	80.4	80.8	88.1	89.3	89.4	89.1	91.9	92.0	91.8
	TAHCD	85.6	85.7	82.4	87.7	88.1	93.2	92.8	92.8	92.6	93.2	93.4	93.2
$\eta = 0$ $\epsilon = 5$	MD [5]	78.3	77.4	69.0	75.5	79.0	83.2	90.1	90.1	90.2	92.2	92.5	92.4
	MLCLNet [39]	77.0	76.6	70.8	74.1	78.5	82.5	86.4	86.5	86.3	88.7	88.5	88.7
	QMF [7]	76.4	75.8	71.0	70.8	75.0	78.9	86.5	86.5	86.4	91.2	91.7	91.7
	PDF [8]	76.0	73.6	67.4	68.9	73.6	78.6	88.2	88.2	88.2	89.2	90.1	90.1
	NCR [43]	71.5	66.8	53.0	67.9	71.7	70.4	82.0	81.8	81.9	88.0	89.1	89.1
	ALBEF [44]	71.2	66.5	52.6	68.2	71.9	70.6	81.7	81.8	81.8	87.6	88.4	88.3
	SMILE [28]	71.5	67.0	54.3	67.6	72.3	71.1	82.0	81.9	81.9	89.7	90.1	90.0
	SPS [29]	72.1	67.4	54.7	70.2	74.5	75.2	83.4	83.2	83.6	90.5	90.7	90.5
	TAHCD	84.4	84.0	80.0	81.1	81.1	85.6	92.8	92.8	92.6	93.0	93.1	93.1
$\eta = 10\%$ $\epsilon = 0$	MD [5]	70.8	69.7	54.5	72.6	73.9	78.1	69.4	69.3	68.3	73.1	73.2	73.2
	MLCLNet [39]	70.4	68.2	50.5	70.4	70.6	76.2	69.2	68.8	68.1	73.2	73.9	74.0
	QMF [7]	68.8	64.9	50.3	70.8	69.3	73.1	70.3	70.2	69.5	73.4	74.3	74.3
	PDF [8]	65.0	56.7	41.7	67.9	72.8	77.3	69.4	69.3	69.0	74.1	74.2	74.2
	NCR [43]	69.6	65.4	51.1	69.8	70.9	76.3	65.1	65.3	65.3	72.1	72.3	72.2
	ALBEF [44]	69.1	65.2	50.8	70.0	73.1	77.6	65.8	65.7	65.7	72.4	72.3	72.3
	SMILE [28]	68.9	64.6	50.2	69.1	70.0	77.4	62.2	62.3	61.9	73.2	73.4	73.4
	SPS [29]	71.6	71.1	58.2	74.2	75.5	81.3	71.6	71.2	71.9	74.1	74.4	74.4
	TAHCD	73.4	73.0	69.4	79.2	79.6	83.5	73.0	73.3	72.6	75.5	75.6	75.6
$\eta = 10\%$ $\epsilon = 5$	MD [5]	65.8	58.5	42.4	68.9	72.7	72.3	68.5	67.9	67.2	73.3	73.4	73.4
	MLCLNet [39]	65.1	58.2	42.1	64.9	70.1	71.5	67.6	67.7	68.3	72.9	72.8	73.1
	QMF [7]	65.0	58.9	44.4	62.2	69.2	70.1	64.8	65.1	64.8	73.2	73.7	73.7
	PDF [8]	60.5	48.1	31.0	66.0	72.7	72.1	68.5	68.0	67.8	72.2	72.9	72.9
	NCR [43]	64.2	65.0	45.2	64.7	70.2	68.0	67.1	67.1	67.9	72.0	72.8	72.8
	ALBEF [44]	67.9	66.0	48.3	68.3	71.1	70.8	69.4	69.6	69.4	72.3	72.4	72.2
	SMILE [28]	66.8	65.9	47.8	68.4	68.9	70.2	56.8	56.4	55.9	70.8	71.3	71.2
	SPS [29]	68.1	66.2	48.3	69.2	72.4	71.3	70.2	70.1	70.9	72.8	72.8	72.5
	TAHCD	69.2	67.9	60.1	76.4	78.6	77.2	73.0	73.0	72.4	75.3	75.1	75.2

IV. EXPERIMENTS

In this section, we conduct extensive experiments to validate the robustness and generalization ability of the proposed Test-time Adaptive Hierarchical Co-enhanced Denoising Network (TAHCD) under multimodal noise. Experimental Setups are first introduced in Sec. IV-A. Comparisons with state-of-the-art methods and ablation studies are then presented in Secs. IV-B and IV-C, respectively. Discussions on different model components, together with parameter analyses and additional investigations, are detailed in Secs. IV-D–IV-G.

A. Experimental Settings

1) **Datasets:** Experiments are conducted on four commonly used multimodal datasets in previous works [5], [7], [21], [22], [24], [39], [46]. (1) **BRCA:** BRCA [47] is a dataset for breast invasive carcinoma PAM50 subtype classification. The dataset comprises 875 samples, with each sample containing features from three modalities: mRNA expression data (mRNA), DNA methylation data (meth), and miRNA expression data (miRNA). These samples are categorized into five subtypes: Normal-like, Basal-like, HER2-enriched,

Luminal A, and Luminal B, with 115, 131, 46, 435, and 147 samples, respectively. BCRA can be obtained from The Cancer Genome Atlas program (TCGA)¹. (2) **ROSMAP:** ROSMAP [48]–[50] is a dataset containing samples from Alzheimer’s patients and normal control subjects. The dataset consists of 351 samples, including 182 Alzheimer’s disease patients and 169 normal control samples. Each sample includes data from three modalities: mRNA expression data (mRNA), DNA methylation data (meth), and miRNA expression data (miRNA). (3) **CUB:** Caltech-UCSD Birds dataset [51] comprises 200 categories of birds. It contains a total of 11,788 samples, with each sample including data from two modalities: images of birds and their corresponding textual descriptions. (4) **UPMC FOOD101:** The UPMC FOOD101 dataset [52] comprises food images from 101 categories obtained through Google Image search and corresponding textual descriptions. This dataset contains 90,704 samples, where each sample’s image and text are collected from uncontrolled environments, thus inherently containing noise.

¹<https://www.cancer.gov/aboutnci/organization/ccg/research/structuralgenomics/tcga>

TABLE II

COMPARISON OF CLASSIFICATION PERFORMANCE BETWEEN THE PROPOSED TAHCD AND OTHER RELIABLE MULTIMODAL CLASSIFICATION METHODS ON THE BRCA, ROSMAP, CUB, AND UPMC FOOD101 DATASETS. ALL METHODS ARE TRAINED ON THE ORIGINAL DATASETS AND TEST ON DATA CORRUPTED WITH MULTIMODAL NOISE ($\eta = 10\%$, $\epsilon = 5$).

Methods	BRCA			ROSMAP			CUB			FOOD101		
	ACC	WeightedF1	MacroF1	ACC	F1	AUC	ACC	WeightedF1	MacroF1	ACC	WeightedF1	MacroF1
MD [5]	51.4	50.8	44.3	58.6	58.5	57.3	57.4	57.7	57.6	58.1	57.8	57.8
MLCLNet [39]	49.6	48.7	42.1	56.7	56.1	54.8	54.8	54.9	54.9	55.4	55.7	55.7
QMF [7]	56.2	55.8	49.3	64.4	64.6	65.5	61.5	61.3	61.1	63.6	63.7	63.6
PDF [8]	56.6	56.4	49.9	65.1	65.3	66.3	62.2	62.3	62.4	64.4	64.8	64.7
NCR [43]	45.8	44.6	39.2	53.2	53.0	54.3	49.5	49.4	49.2	51.4	51.3	51.3
ALBEF [44]	45.5	44.3	39.0	53.3	53.2	54.6	49.2	49.2	49.1	51.2	51.1	51.2
SMILE [28]	45.0	44.1	38.7	52.8	52.8	53.5	49.2	49.1	49.1	50.7	50.8	50.8
SPS [29]	46.1	45.3	40.1	56.6	56.9	57.1	52.1	52.1	52.7	55.9	56.1	56.0
TAHCD	67.4	66.2	59.2	75.1	77.3	76.4	72.4	72.4	71.8	74.2	74.1	74.1

TABLE III

ABLATION STUDIES ON FOUR DATASETS WITH NOISE ($\eta = 10\%$, $\epsilon = 5$) ADDED ON BOTH TRAINING AND TEST DATA

Dataset	ASSA	SACA	TTCE	ACC	WeightedF1	MacroF1
BRCA	✓	✓	✓	69.2	67.9	60.1
	✓	✓	✗	67.4	65.6	58.4
	✓	✗	✗	65.8	64.0	56.5
	✗	✗	✗	48.3	47.1	45.5
CUB	✓	✓	✓	73.0	73.0	72.4
	✓	✓	✗	71.3	71.3	71.0
	✓	✗	✗	69.8	69.7	69.7
	✗	✗	✗	58.6	58.4	58.6
FOOD101	✓	✓	✓	75.3	75.1	75.2
	✓	✓	✗	74.7	74.6	74.7
	✓	✗	✗	72.3	72.4	72.3
	✗	✗	✗	60.8	60.6	60.9
Dataset	ASSA	SACA	TTCE	ACC	F1	AUC
ROSMAP	✓	✓	✓	76.4	78.6	77.2
	✓	✓	✗	74.6	76.1	76.2
	✓	✗	✗	72.7	73.8	74.0
	✗	✗	✗	53.1	52.7	53.8

2) *Compared Methods*: To validate the reliability of TAHCD under multimodal noise, we compare it with several representative reliable multimodal learning methods in our experiments, including multimodal dynamics (**MD**) [5], multi-level confidence learning (**MLCLNet**) [39], quality-aware multimodal fusion (**QMF**) [7], predictive dynamic fusion (**PDF**) [8], Noisy Correspondence Rectifier (**NCR**) [43], Align before Fuse (**ALBEF**) [44], Semantic Invariance Learning (**SMILE**) [28], and Seeking Proxy Point via Stable Feature Space (**SPS**) [29]. The first four methods focus on learning high-confidence modality representations or fusing different modalities based on their qualities, and are therefore regarded as representative approaches for modality-specific noise removal. The remaining four methods emphasize learning cross-modality consistency and correspondence, and are thus treated as representative approaches for cross-modality noise removal.

3) Evaluation Metrics:

a) *BRCA & CUB & UPMC FOOD101*: BRCA, CUB and UPMC FOOD101 provide multi-class classification task. Three metrics, including accuracy (ACC), average F1 score weighted by support (WeightedF1), and macro-averaged F1 score (MacroF1), are employed to evaluate the performance

of different methods.

b) *ROSMAP*: ROSMAP provides a binary classification task. The accuracy (ACC), F1 score (F1), and area under the receiver operating characteristic curve (AUC) of different methods are reported by experiment.

4) Implementation Details:

a) *Training Details*: We implement the proposed method and other compared methods on the PyTorch 1.12.0 and cuda 11.6 platform, running on Ubuntu 20.04.2 LTS, utilizing one GPU (NVIDIA RTX A6000 with 48 GB of memory) and CPU of AMD EPYC 75F3. The Adam optimizer with learning rate decay is employed to train the model. The initial learning rate of the Adam optimizer is set to 1e-4, the weight decay is set to 1e-4, and the multiplicative factor of the learning rate decay is set to 0.2. All the quantitative results of the proposed TAHCD are the average of five random seeds.

b) *Model Implementation Details*: To evaluate the classification performance of **NCR** [43] and **ALBEF** [44], the sample features after being filtered or rectified are utilized to train the classifier. For **SMILE** [28] and **SPS** [29], the sample features output by its well-trained encoders are used for classification.

c) *Experimental Details*: Two types of noise are involved in the experiments: modality-specific and cross-modality noise. The modality-specific noise is implemented following previous works [8], [21], [24], and ϵ is its severity level. The implementation of cross-modality noise follows SMILE [28], where unaligned samples are introduced by shuffling the features of each modality for a random subset of samples with a proportion of η .

B. Comparison with State-of-the-Art Methods

To demonstrate the improved robustness and generalization ability of the proposed TAHCD under multimodal noise, we conduct comparative experiments on datasets corrupted by modality-specific and cross-modality noise, following previous works [5], [8], [28]. ϵ and η represent the severity levels of modality-specific and cross-modality noise, respectively.

1) *Robustness*: To evaluate the improved robustness of TAHCD against multimodal noise, we compare the classification performance of different methods on training and test sets that are both corrupted by the same noise, as reported

TABLE IV

ABLATION STUDIES ON FOUR DATASETS WITH TRAINING ON ORIGINAL DATA AND TESTING UNDER NOISE ADDED DATA ($\eta = 10\%$, $\epsilon = 5$).

Dataset	ASSA	SACA	TTCE	ACC	WeightedF1	MacroF1
BRCA	✓	✓	✓	67.4	66.2	59.2
	✓	✓	✗	50.1	49.8	47.2
	✓	✗	✗	49.2	49.0	45.4
	✗	✗	✗	46.5	46.7	43.1
CUB	✓	✓	✓	72.4	72.4	71.8
	✓	✓	✗	54.6	54.6	53.8
	✓	✗	✗	53.3	53.3	52.7
	✗	✗	✗	51.6	51.4	51.6
FOOD101	✓	✓	✓	74.2	74.1	74.1
	✓	✓	✗	55.6	54.9	55.1
	✓	✗	✗	54.3	54.3	54.3
	✗	✗	✗	51.9	51.8	52.1
Dataset	ASSA	SACA	TTCE	ACC	F1	AUC
ROSMAP	✓	✓	✓	75.1	77.3	76.4
	✓	✓	✗	56.3	57.4	55.7
	✓	✗	✗	54.8	55.9	54.8
	✗	✗	✗	52.2	52.3	50.8

in Table I. Methods such as MD, MLCLNet, QMF, and PDF learn reliable modality representations by estimating modality confidence but lack awareness of cross-modality alignment. Consequently, their performance is relatively stable under settings with only modality-specific noise ($\eta = 0$, $\epsilon = 5$), while their performance degrades significantly once cross-modality noise is introduced (all settings with $\eta = 10\%$). For NCR, ALBEF, SMILE, and SPS, these methods primarily focus on cross-modality alignment while paying limited attention to confidence of each modality. As a result, they exhibit relatively stable performance when only cross-modality noise is present ($\eta = 10\%$, $\epsilon = 0$), but their performance degrades noticeably once modality-specific noise is introduced (all settings with $\epsilon = 5$). In contrast, TAHCD consistently achieves more stable performance than the compared methods under various noise conditions on all datasets, demonstrating superior robustness. This advantage primarily stems from its explicit modeling of both modality-specific and cross-modality noise and their joint removal across multiple levels, enabling more thorough noise suppression.

2) *Generalization ability*: To evaluate the improved generalization ability of TAHCD under previously unseen noise, we train all methods on the original datasets and test them on noise-corrupted data. Table II reports the test results on data corrupted by a mixture of modality-specific noise with $\epsilon = 5$ and cross-modality noise with $\eta = 10\%$. When confronted with noise unseen during training, all baseline methods suffer substantial performance degradation. In particular, compared with the results under the noise setting of $\eta = 10\%$ and $\epsilon = 5$ in Table I, their performance degrades substantially, indicating limited adaptability to previously unseen noise during training. In contrast, our TAHCD outperforms other baselines when exposed to previously unseen noise, while exhibiting a noticeably smaller performance degradation compared to the setting where such noise is observed during training. The possible reason is that TAHCD can adapt in response to input noise at test time, thereby exhibiting stronger generalization ability.

C. Ablation Study

To evaluate the overall effectiveness of the three key components of TAHCD, namely Adaptive Stable Subspace Alignment (ASSA), Sample-Adaptive Confidence Alignment (SACA), and Test-Time Cooperative Enhancement (TTCE), we conduct ablation studies. As shown in Table III, following the same setting as Table I, identical noise is added to both the training and test data to assess the contribution of each component to model robustness. The results indicate that all three components contribute to robustness improvement, with ASSA providing the largest gain, followed by SACA and TTCE. A possible reason is that the noise is sampled from a shared distribution and added to all samples, exhibiting strong global characteristics, which allows ASSA to remove most of the noise at the global level. SACA also contributes to performance improvements, indicating that even noise sampled from the same distribution contains outlier components, thereby demonstrating the necessity of instance-level denoising on each sample. The performance gains brought by TTCE indicate that the cooperative enhancement between global-level and instance-level denoising is beneficial for improving denoising effectiveness.

Additionally, to evaluate the contribution of each component to generalization ability, we follow the same setting as in Table II by training the model on the original dataset and testing it on noise-corrupted data. The results are shown in Table IV. Removing TTCE leads to a substantial performance drop, indicating its critical role in adapting to previously unseen noise and improving generalization. When TTCE is removed, further removing ASSA or SACA results in additional performance degradation, indicating that these two components also contribute to learning more generalizable multimodal representations. A possible reason is that ASSA and SACA learn informative modality distribution priors, which help guide the model to better remove unseen noise.

D. Discussion On ASSA

As detailed in Sec. III-B, ASSA learns a mask w_λ^m based on the singular values obtained from the decomposition of modality feature covariance matrices to construct stable feature subspace, guided by two constraints \mathcal{L}_o and \mathcal{L}_a .

1) *Discussion On Adaptive Stable Subspace Construction*: We evaluate the effectiveness of stable subspace construction by examining whether ASSA learns noise-related masks w_λ^m . Specifically, we generate Gaussian noise $n^m \in \mathbb{R}^{N \times d^m}$ with severity $\epsilon = 5$, set the values of half of the feature dimensions in the noise matrix to zero, and add the resulting noise to one modality x^m . We then visualize the learned mask w_λ^m before and after noise corruption in Fig. 3, with results shown for the corrupted image modality on the CUB dataset. Before adding noise (left panel of Fig. 3), the learned mask show small values in few feature dimensions, suggesting that most features of the original high-quality data are informative and largely retained. After the noise is added (right panel of Fig. 3), approximately half of the learned mask values corresponding to corrupted feature dimensions decrease, appearing lighter in the figure. This indicates that ASSA can learn masks highly correlated

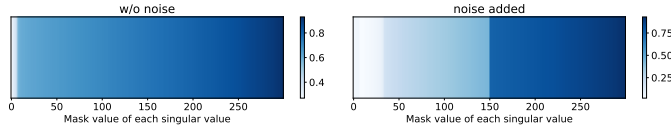


Fig. 3. Visualization of masks w_λ^m learned by ASSA on CUB image features, before and after adding noise ($\epsilon = 5$) to half of the feature dimensions.

TABLE V

EVALUATION OF THE EFFECTS OF \mathcal{L}_o AND \mathcal{L}_a ON DATASETS WITH MODALITY-SPECIFIC NOISE ($\epsilon = 5$).

Dataset	Method	ACC	WeightedF1	MacroF1
BRCA	w/o \mathcal{L}_o	75.1	74.8	70.3
	w/o \mathcal{L}_a	83.8	83.2	79.6
	Proposed	84.4	84.0	80.0
CUB	w/o \mathcal{L}_o	84.4	84.3	84.4
	w/o \mathcal{L}_a	92.4	92.3	92.3
	Proposed	92.8	92.8	92.6
FOOD101	w/o \mathcal{L}_o	87.1	87.0	87.0
	w/o \mathcal{L}_a	92.5	92.4	92.6
	Proposed	93.0	93.0	93.1
Dataset	Method	ACC	F1	AUC
ROSMAP	w/o \mathcal{L}_o	70.4	70.1	72.3
	w/o \mathcal{L}_a	79.8	79.6	84.1
	Proposed	81.1	81.1	85.6

with noise, thereby preserving informative principal axes and ensuring the stability of the constructed feature subspace.

2) *Effectiveness of \mathcal{L}_o and \mathcal{L}_a* : Further experiments are conducted to evaluate the roles of the two constraints \mathcal{L}_o and \mathcal{L}_a in noise removal. We perform ablation studies on datasets corrupted only by modality-specific noise with $\epsilon = 5$ and only by cross-modality noise with $\eta = 10\%$, respectively. As shown in Table V, on datasets with only modality-specific noise ($\epsilon = 5$), removing \mathcal{L}_o causes a much more significant performance drop than removing \mathcal{L}_a . This indicates that \mathcal{L}_o plays a dominant role in guiding modality-specific noise removal. In contrast, as shown in Table VI, on datasets with only cross-modality noise ($\eta = 10\%$), removing \mathcal{L}_a results in a substantially larger performance drop compared to removing \mathcal{L}_o , demonstrating that \mathcal{L}_a primarily guides cross-modality noise removal.

3) *Further Discussion On the Subspace Projection Alignment*: To further verify the effectiveness of Subspace Projection Alignment in aligning projections onto stable feature subspaces, we add cross-modality noise with varying intensity η on data with modality-specific noise $\epsilon = 5$. We compare two strategies: aligning directly on modality features (w/o projection) and aligning projections onto stable subspaces via Subspace Projection Alignment (with projection). As shown in Table VII, under modality-specific noise, the “with projection” strategy exhibits stronger robustness than “w/o projection” as cross-modality noise increases. This indicates that aligning modality projections within their respective stable subspaces enables more effective suppression of cross-modality noise in the presence of modality-specific corruption.

TABLE VI
EVALUATION OF THE EFFECTS OF \mathcal{L}_o AND \mathcal{L}_a ON DATASETS WITH CROSS-MODALITY NOISE ($\eta = 10\%$).

Dataset	Method	ACC	WeightedF1	MacroF1
BRCA	w/o \mathcal{L}_o	71.5	71.2	70.3
	w/o \mathcal{L}_a	59.7	59.1	57.8
	Proposed	73.4	73.0	69.4
CUB	w/o \mathcal{L}_o	71.3	71.6	71.6
	w/o \mathcal{L}_a	60.1	60.3	60.2
	Proposed	73.0	73.3	72.6
FOOD101	w/o \mathcal{L}_o	73.4	73.3	73.3
	w/o \mathcal{L}_a	61.7	61.4	61.5
	Proposed	75.5	75.6	75.6
Dataset	Method	ACC	F1	AUC
ROSMAP	w/o \mathcal{L}_o	77.4	77.2	82.7
	w/o \mathcal{L}_a	55.2	55.4	57.1
	Proposed	79.2	79.6	83.5

TABLE VII
EFFECTIVENESS OF ALIGNMENT ON PROJECTIONS ONTO STABLE FEATURE SUBSPACES UNDER CROSS-MODALITY NOISE WITH VARYING η (WITH MODALITY-SPECIFIC NOISE $\epsilon = 5$).

Dataset	Method	$\eta = 0$	$\eta = 10\%$	$\eta = 20\%$
BRCA	w/o projection	84.1	65.2	54.8
	with projection	85.6	73.4	65.8
ROSMAP	w/o projection	85.6	74.1	60.3
	with projection	87.7	79.2	71.8
CUB	w/o projection	91.5	68.8	57.9
	with projection	92.8	73.0	66.2
FOOD101	w/o projection	92.0	70.2	59.6
	with projection	93.2	75.5	68.4

E. Discussion On SACA

1) *Effectiveness of Noise Experts*: More experiments are conducted to verify that the modality specific noise experts and cross modality noise experts in SACA respectively facilitate the removal of instance level modality-specific and cross-modality noise. Specifically, we first introduce only modality-specific noise $\epsilon = 5$ into one modality of the dataset and visualize the sample masks w_s^m learned by the corresponding modality-specific noise expert. Fig. 5 illustrates the masks learned by the modality-specific noise expert on the image modality affected by noise in the CUB dataset. In the noise-free setting (left), the mask values exhibit strong consistency across samples. After modality-specific noise is added (right), the learned mask show increased variability between samples, reflecting the instance-level diversity of the modality-specific noise and demonstrating that the modality-specific noise expert effectively captures the noise for each sample. Also, we introduce cross-modality noise with $\eta = 20\%$ to one modality of the dataset by randomly shuffling the features of 20% of its samples. Fig. 6 shows the masks learned by the cross-modality noise expert on the image modality affected by noise in the CUB dataset. Before noise is added (left), the masks of different samples exhibit a relatively consistent pattern, whereas after noise introduction (right), the masks

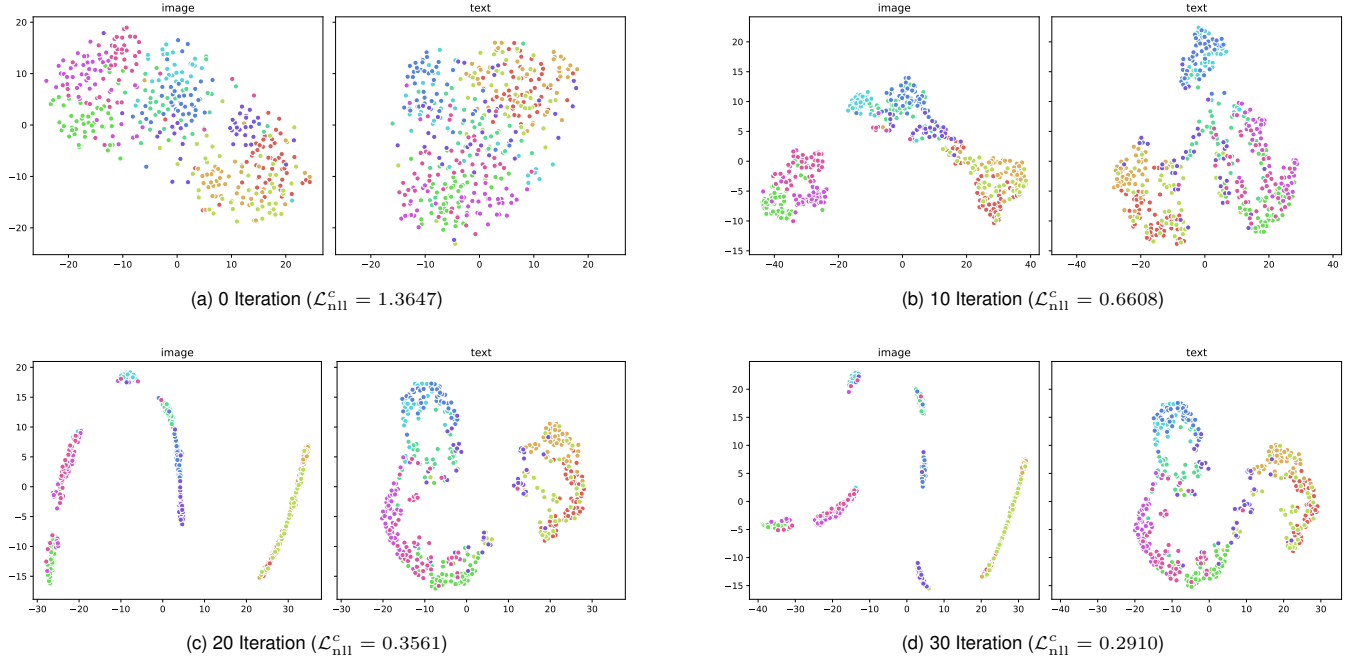


Fig. 4. T-SNE visualization of the learned modality representations and the value of cross-modality alignment loss $\mathcal{L}_{\text{nll}}^c$ results on the CUB dataset with both modalities corrupted by modality-specific and cross-modality noise ($\epsilon = 5, \eta = 10\%$) after different TTCE co-enhancement iterations. Points in different colors represent sample representations from different classes.

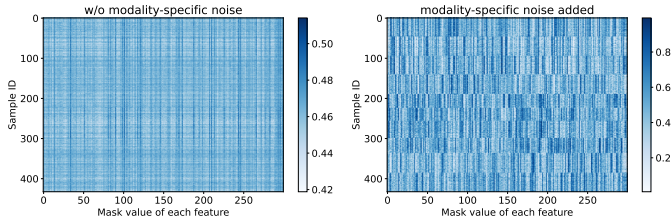


Fig. 5. Visualization of sample-wise masks learned by the modality-specific noise expert on the corrupted image modality of CUB, before and after adding modality-specific noise ($\epsilon = 5$).

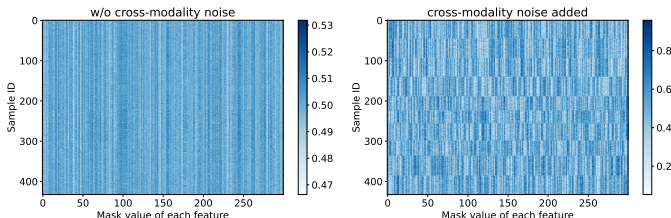


Fig. 6. Visualization of sample-wise masks learned by the cross-modality noise expert on the corrupted image modality of CUB, before and after adding cross-modality noise ($\eta = 10\%$).

show substantial variability across samples. This demonstrates that the cross-modality noise expert can effectively capture sample-specific corrupted information introduced by noise.

2) *Discussion on Confidence-Aware Asymmetric Slack Alignment:* We first conduct experiments to validate the effectiveness of the slack alignment proposed in Confidence-Aware Asymmetric Slack Alignment. Specifically, we compare with existing methods that enforce cross-modality consistency, including similarity-based approaches (sim), as used in [29],

[43], [44], and information-theoretic approaches (MI), as used in [28]. “slack” represents applying our $\mathcal{L}_{\text{nll}}^c$ that retains the slack-alignment mechanism while removing modality-confidence guidance. As shown in Table VIII, under cross-modality noise with varying intensity η , our slack alignment exhibits stronger stability than other methods, indicating superior robustness. “MI” achieves better performance than “sim”, likely due to its less restrictive constraint on cross-modality consistency.

We also conduct experiment to validate the effectiveness of incorporating modality confidence to guide slack alignment. Specifically, the model is trained on data with modality-specific and cross-modality noise ($\epsilon = 1, \eta = 10\%$), and the changes in modality-wise confidence and the loss $\mathcal{L}_{\text{nll}}^c$ are reported for both with and without confidence guidance. The variant without confidence guidance is implemented by removing the gradient modulation in Eq. (13). Modality confidence reported in Fig. 7 is computed as the average of the likelihoods $p^m(\hat{h}_{s,i}^m)$ of all sample representations $\hat{h}_{s,i}^m$ under the corresponding modality-specific feature prior p^m . As shown in the left panel of Fig. 7, as training progresses, the confidence of each modality gradually increases, indicating progressive noise removal. Moreover, with modality-confidence guidance, modality confidence rises to higher levels than without such guidance, suggesting that confidence guidance promotes alignment toward high-confidence features across modalities, thereby yielding more robust representations. Moreover, as shown in the right panel of Fig. 7, the loss $\mathcal{L}_{\text{nll}}^c$ decreases faster with confidence guidance than without it, indicating that confidence guidance also accelerates the alignment process.

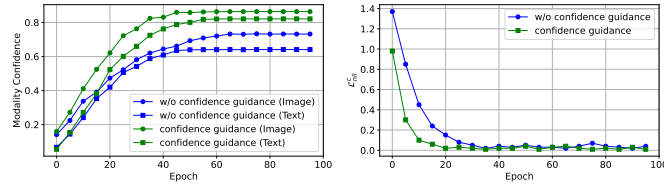


Fig. 7. Changes in modality-wise confidence and the decline of $\mathcal{L}_{\text{nnl}}^c$ during training on the FOOD101 dataset with cross-modality noise ($\eta = 10\%$) and modality-specific noise ($\epsilon = 1$), under two conditions: with and without the guidance of modality confidence on slack alignment.

TABLE VIII
COMPARISON OF MODEL PERFORMANCE UNDER NOISE USING DIFFERENT CROSS-MODALITY ALIGNMENT METHODS.

Dataset	Method	$\eta = 0$	$\eta = 10\%$	$\eta = 20\%$
BRCA	sim	84.6	66.8	57.3
	MI	85.0	70.8	61.3
	slack	85.6	73.4	65.8
ROSMAP	sim	86.2	75.3	62.8
	MI	86.9	76.4	65.1
	slack	87.7	79.2	71.8
CUB	sim	92.0	69.8	60.5
	MI	92.3	70.6	62.7
	slack	92.8	73.0	66.2
FOOD101	sim	92.5	71.3	61.8
	MI	93.0	72.6	64.1
	slack	93.2	75.5	68.4

F. Discussion On TTCE

To verify that TTCE effectively enhances the model's adaptability and generalization to previously unseen noise, we conduct experiments using the original training data and test data corrupted with modality-specific and cross-modality noise ($\eta = 10\%$, $\epsilon = 5$). The model is first trained, and then the representations $\hat{h}_s^m + \hat{h}_c^m$ of each modality during the iterative enhancement of TTCE on the noisy test data are visualized. As shown in Fig. 4, before TTCE iterations (0 iteration), the learned representations exhibit poor intra-modality class separability and weak cross-modality alignment (high $\mathcal{L}_{\text{nnl}}^c$), indicating insufficient removal of newly encountered noise. As TTCE proceeds, intra-modality class separability gradually improves, and cross-modality alignment is substantially enhanced ($\mathcal{L}_{\text{nnl}}^c$ decreases), indicating that newly introduced modality-specific and cross-modality noise is progressively removed. These results demonstrate that, through multiple TTCE updates, the model can progressively adapt to and remove noise unseen in training stage, thereby achieving stronger generalization performance.

G. Parameter Analysis

More experiments are conducted to analyze the hyperparameters of the proposed model. In these experiments, TAHCD is trained on the original dataset and test on data with modality-specific noise ($\epsilon = 5$) and cross-modality noise ($\eta = 10\%$). TAHCD mainly involves three hyperparameters, namely the update ratios α and β for μ and Σ in Eq. (17), and the number of update iterations E in TTCE. The values of α and β lie

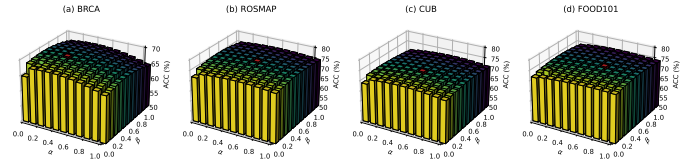


Fig. 8. Variation of test accuracy under different values of α and β .

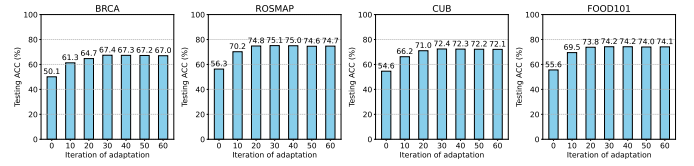


Fig. 9. Analysis of TTCE iteration number E on four datasets.

in $[0, 1]$, indicating the extent to which the modality feature distributions incorporate the newly estimated mean and covariance. Setting $\alpha = \beta = 0$ means that the distributions are not updated, while $\alpha = \beta = 1$ indicates that the newly computed statistics fully replace the original ones. As shown in Fig. 8, increasing α and β leads to a model classification accuracy trend that first improves and then degrades. The α and β values that achieve the best performance are relatively consistent across datasets, for example, $\alpha = 0.4$ and $\beta = 0.3$ on BRCA, and $\alpha = 0.4$ and $\beta = 0.4$ on ROSMAP. Additionally, Fig. 9 shows that as the number of update iterations E increases, the test accuracy first rises and generally stabilizes around $E = 30$ across all datasets. This indicates that the model has completed its adaptive adjustment to the noise present in the current test data. When the noise severity increases, more update iterations are required, and the optimal value of E corresponding to the highest accuracy increases accordingly.

V. CONCLUSION

Existing multimodal learning methods struggle to achieve robust multimodal representation learning under heterogeneous noise and exhibit limited adaptability and generalization to unseen noise. To address these challenges, we propose the Test-time Adaptive Hierarchical Co-enhanced Denoising Network (TAHCD). TAHCD introduces Adaptive Stable Subspace Alignment and Sample-Adaptive Confidence Alignment to jointly remove modality-specific and cross-modality noise at the global and instance levels, respectively, thereby improving robustness. In addition, TAHCD designs a test-time cooperative enhancement mechanism that enables collaborative enhancement between global-level and instance-level denoising processes driven by input sample noise in a label-free manner. This enables TAHCD to adapt more effectively to unseen noise at test time, improving the model's generalization ability. Experiments on multiple benchmarks demonstrate that TAHCD outperforms other state-of-the-art reliable multimodal learning methods in robustness and generalization ability.

Although existing reliable multimodal learning methods have been extensively studied for classification tasks, their reliability in other machine learning tasks, such as regression and semantic segmentation, remains insufficiently explored.

This presents a promising and important direction for further investigation. Accordingly, future work will extend and validate the proposed approach across a broader set of machine learning tasks.

REFERENCES

- [1] M. Ma, W. Ma, L. Jiao, X. Liu, F. Liu, L. Li, and S. Yang, "Mbsinet: Multimodal balanced self-learning interaction network for image classification," *IEEE Transactions on Circuits and Systems for Video Technology*, vol. 34, no. 5, pp. 3819–3833, 2024.
- [2] Z. Zhang, C. P. Chen, Z. Su, and T. Zhang, "Prompts libra: Enhanced image outpainting diffusion model with balanced bimodal guidance," *IEEE Transactions on Circuits and Systems for Video Technology*, 2025.
- [3] P. P. Liang, A. Zadeh, and L.-P. Morency, "Foundations and trends in multimodal machine learning: Principles, challenges, and open questions," *arXiv preprint arXiv:2209.03430*, 2022.
- [4] T. Baltrušaitis, C. Ahuja, and L.-P. Morency, "Multimodal machine learning: A survey and taxonomy," *IEEE transactions on pattern analysis and machine intelligence*, vol. 41, no. 2, pp. 423–443, 2018.
- [5] Z. Han, F. Yang, J. Huang, C. Zhang, and J. Yao, "Multimodal dynamics: Dynamical fusion for trustworthy multimodal classification," in *Proceedings of the IEEE/CVF conference on computer vision and pattern recognition*, 2022, pp. 20707–20717.
- [6] X. Zou, C. Tang, X. Zheng, Z. Li, X. He, S. An, and X. Liu, "Dpnet: Dynamic poly-attention network for trustworthy multi-modal classification," in *Proceedings of the 31st ACM International Conference on Multimedia*, 2023, pp. 3550–3559.
- [7] Q. Zhang, H. Wu, C. Zhang, Q. Hu, H. Fu, J. T. Zhou, and X. Peng, "Provable dynamic fusion for low-quality multimodal data," in *International conference on machine learning*. PMLR, 2023, pp. 41753–41769.
- [8] B. Cao, Y. Xia, Y. Ding, C. Zhang, and Q. Hu, "Predictive dynamic fusion," in *Forty-first International Conference on Machine Learning*, 2024. [Online]. Available: <https://openreview.net/forum?id=LYpGLrC4oq>
- [9] X. Dong, H. Zhang, L. Zhu, L. Nie, and L. Liu, "Hierarchical feature aggregation based on transformer for image-text matching," *IEEE Transactions on Circuits and Systems for Video Technology*, vol. 32, no. 9, pp. 6437–6447, 2022.
- [10] Z. Li, Q. Lin, H. Fan, T. Zhao, and D. Zhang, "Siavc: Semi-supervised framework for industrial accident video classification," *IEEE Transactions on Circuits and Systems for Video Technology*, vol. 35, no. 3, pp. 2603–2615, 2025.
- [11] M. Jubran, A. Abbas, A. Chadha, and Y. Andreopoulos, "Rate-accuracy trade-off in video classification with deep convolutional neural networks," *IEEE Transactions on Circuits and Systems for Video Technology*, vol. 30, no. 1, pp. 145–154, 2020.
- [12] M. Li, W. Gong, P. Yan, X. Li, Y. Jiang, H. Luo, H. Zhou, and S. Yin, "Joint lesion detection and classification of breast ultrasound video via a clinical knowledge-aware framework," *IEEE Transactions on Circuits and Systems for Video Technology*, vol. 35, no. 1, pp. 45–61, 2025.
- [13] M. Ren, X. Huang, J. Liu, M. Liu, X. Li, and A.-A. Liu, "Mah: Multimodal adversarial learning network for conversational emotion recognition," *IEEE Transactions on Circuits and Systems for Video Technology*, vol. 33, no. 11, pp. 6965–6980, 2023.
- [14] M. Ren, X. Huang, J. Liu, Z. Gao, Y. Su, and A.-A. Liu, "Kamin: Knowledge-aware multimodal interaction network for emotion recognition in conversation," *IEEE Transactions on Circuits and Systems for Video Technology*, vol. 35, no. 8, pp. 8344–8358, 2025.
- [15] F. Qi, H. Zhang, X. Yang, and C. Xu, "A versatile multimodal learning framework for zero-shot emotion recognition," *IEEE Transactions on Circuits and Systems for Video Technology*, vol. 34, no. 7, pp. 5728–5741, 2024.
- [16] Q. Zhang, Y. Wei, Z. Han, H. Fu, X. Peng, C. Deng, Q. Hu, C. Xu, J. Wen, D. Hu *et al.*, "Multimodal fusion on low-quality data: A comprehensive survey," *arXiv preprint arXiv:2404.18947*, 2024.
- [17] L. Zhang, X. Zhu, X. Chen, X. Yang, Z. Lei, and Z. Liu, "Weakly aligned cross-modal learning for multispectral pedestrian detection," in *Proceedings of the IEEE/CVF international conference on computer vision*, 2019, pp. 5127–5137.
- [18] S. Changpinyo, P. Sharma, N. Ding, and R. Soricul, "Conceptual 12m: Pushing web-scale image-text pre-training to recognize long-tail visual concepts," in *Proceedings of the IEEE/CVF conference on computer vision and pattern recognition*, 2021, pp. 3558–3568.
- [19] D. Feng, L. Rosenbaum, and K. Dietmayer, "Towards safe autonomous driving: Capture uncertainty in the deep neural network for lidar 3d vehicle detection," in *2018 21st international conference on intelligent transportation systems (ITSC)*. IEEE, 2018, pp. 3266–3273.
- [20] T. Nair, D. Precup, D. L. Arnold, and T. Arbel, "Exploring uncertainty measures in deep networks for multiple sclerosis lesion detection and segmentation," *Medical image analysis*, vol. 59, p. 101557, 2020.
- [21] H. Zhou, Z. Xue, Y. Liu, B. Li, J. Du, M. Liang, and Y. Qi, "Calm: An enhanced encoding and confidence evaluating framework for trustworthy multi-view learning," in *Proceedings of the 31st ACM International Conference on Multimedia*, 2023, pp. 3108–3116.
- [22] Z. Han, C. Zhang, H. Fu, and J. T. Zhou, "Trusted multi-view classification," in *International Conference on Learning Representations*, 2020.
- [23] ———, "Trusted multi-view classification with dynamic evidential fusion," *IEEE transactions on pattern analysis and machine intelligence*, vol. 45, no. 2, pp. 2551–2566, 2022.
- [24] Y. Geng, Z. Han, C. Zhang, and Q. Hu, "Uncertainty-aware multi-view representation learning," in *Proceedings of the AAAI Conference on Artificial Intelligence*, vol. 35, no. 9, 2021, pp. 7545–7553.
- [25] R. Huang, Y. Long, J. Han, H. Xu, X. Liang, C. Xu, and X. Liang, "Nlip: Noise-robust language-image pre-training," in *Proceedings of the AAAI Conference on Artificial Intelligence*, vol. 37, no. 1, 2023, pp. 926–934.
- [26] X. Li, X. Yin, C. Li, P. Zhang, X. Hu, L. Zhang, L. Wang, H. Hu, L. Dong, F. Wei *et al.*, "Oscar: Object-semantics aligned pre-training for vision-language tasks," in *Computer Vision–ECCV 2020: 16th European Conference, Glasgow, UK, August 23–28, 2020, Proceedings, Part XXXI*. Springer, 2020, pp. 121–137.
- [27] R. Nakada, H. I. Gulluk, Z. Deng, W. Ji, J. Zou, and L. Zhang, "Understanding multimodal contrastive learning and incorporating unpaired data," in *International Conference on Artificial Intelligence and Statistics*. PMLR, 2023, pp. 4348–4380.
- [28] P. Zeng, M. Yang, Y. Lu, C. Zhang, P. Hu, and X. Peng, "Semantic invariant multi-view clustering with fully incomplete information," *IEEE Transactions on Pattern Analysis and Machine Intelligence*, 2023.
- [29] Y. Xie, S. Cai, T. Tong, P. Hu, and X. Zhu, "Seeking proxy point via stable feature space for noisy correspondence learning," in *Proceedings of the Thirty-Fourth International Joint Conference on Artificial Intelligence*, 2025, pp. 2072–2080.
- [30] D. Ramachandram and G. W. Taylor, "Deep multimodal learning: A survey on recent advances and trends," *IEEE signal processing magazine*, vol. 34, no. 6, pp. 96–108, 2017.
- [31] Y. Zhu, Y. Wu, N. Sebe, and Y. Yan, "Vision+ x: A survey on multimodal learning in the light of data," *IEEE Transactions on Pattern Analysis and Machine Intelligence*, 2024.
- [32] L. Hang, Y. Fan, X. Xiaohan *et al.*, "Multi-modal multi-instance learning using weakly correlated histopathological images and tabular clinical information in medical image computing and computer assisted intervention–miccai 2021: 24th international conference, strasbourg, france, september 27–october 1, 2021," *Proceedings, Part VIII*, vol. 24, pp. 529–539 Springer, 2021.
- [33] J. Huang, J. Tao, B. Liu, Z. Lian, and M. Niu, "Multimodal transformer fusion for continuous emotion recognition," in *ICASSP 2020–2020 IEEE International Conference on Acoustics, Speech and Signal Processing (ICASSP)*. IEEE, 2020, pp. 3507–3511.
- [34] Y. Li, L. Fan, Y. Liu, Z. Huang, Y. Chen, N. Wang, and Z. Zhang, "Fully sparse fusion for 3d object detection," *IEEE Transactions on Pattern Analysis and Machine Intelligence*, vol. 46, no. 11, pp. 7217–7231, 2024.
- [35] C. Lee and M. Van der Schaar, "A variational information bottleneck approach to multi-omics data integration," in *International Conference on Artificial Intelligence and Statistics*. PMLR, 2021, pp. 1513–1521.
- [36] T. Wang, W. Shao, Z. Huang, H. Tang, J. Zhang, Z. Ding, and K. Huang, "Mogonet integrates multi-omics data using graph convolutional networks allowing patient classification and biomarker identification," *Nature communications*, vol. 12, no. 1, p. 3445, 2021.
- [37] Y. Wang, F. Sun, W. Huang, F. He, and D. Tao, "Channel exchanging networks for multimodal and multitask dense image prediction," *IEEE Transactions on Pattern Analysis and Machine Intelligence*, vol. 45, no. 5, pp. 5481–5496, 2023.
- [38] M. Federici, A. Dutta, P. Forré, N. Kushman, and Z. Akata, "Learning robust representations via multi-view information bottleneck," in *International Conference on Learning Representations*, 2020. [Online]. Available: <https://openreview.net/forum?id=B1xwcyHFDr>
- [39] X. Zheng, C. Tang, Z. Wan, C. Hu, and W. Zhang, "Multi-level confidence learning for trustworthy multimodal classification," in *Proceedings of the AAAI Conference on Artificial Intelligence*, vol. 37, no. 9, 2023, pp. 11381–11389.

- [40] F. Radenovic, A. Dubey, A. Kadian, T. Mihaylov, S. Vandenbende, Y. Patel, Y. Wen, V. Ramanathan, and D. Mahajan, “Filtering, distillation, and hard negatives for vision-language pre-training,” in *Proceedings of the IEEE/CVF conference on computer vision and pattern recognition*, 2023, pp. 6967–6977.
- [41] S. Y. Gadre, G. Ilharco, A. Fang, J. Hayase, G. Smyrnis, T. Nguyen, R. Marten, M. Wortsman, D. Ghosh, J. Zhang *et al.*, “Datacomp: In search of the next generation of multimodal datasets,” *Advances in Neural Information Processing Systems*, vol. 36, 2024.
- [42] P. Sharma, N. Ding, S. Goodman, and R. Soricut, “Conceptual captions: A cleaned, hypernymed, image alt-text dataset for automatic image captioning,” in *Proceedings of the 56th Annual Meeting of the Association for Computational Linguistics (Volume 1: Long Papers)*, 2018, pp. 2556–2565.
- [43] Z. Huang, G. Niu, X. Liu, W. Ding, X. Xiao, H. Wu, and X. Peng, “Learning with noisy correspondence for cross-modal matching,” *Advances in Neural Information Processing Systems*, vol. 34, pp. 29406–29419, 2021.
- [44] J. Li, R. Selvaraju, A. Gotmare, S. Joty, C. Xiong, and S. C. H. Hoi, “Align before fuse: Vision and language representation learning with momentum distillation,” *Advances in neural information processing systems*, vol. 34, pp. 9694–9705, 2021.
- [45] J. Li, D. Li, C. Xiong, and S. Hoi, “Blip: Bootstrapping language-image pre-training for unified vision-language understanding and generation,” in *International conference on machine learning*. PMLR, 2022, pp. 12888–12900.
- [46] B. Cao, Y. Xia, Y. Ding, C. Zhang, and Q. Hu, “Predictive dynamic fusion,” in *Proceedings of the 41st International Conference on Machine Learning*, ser. Proceedings of Machine Learning Research, R. Salakhutdinov, Z. Kolter, K. Heller, A. Weller, N. Oliver, J. Scarlett, and F. Berkenkamp, Eds., vol. 235. PMLR, 21–27 Jul 2024, pp. 5608–5628. [Online]. Available: <https://proceedings.mlr.press/v235/cao24c.html>
- [47] W. Lingle *et al.*, “The cancer genome atlas breast invasive carcinoma collection (tcga-brca)(version 3)[data set]. cancer imag. arch.(2016).”
- [48] S. Mukherjee, S. Walter, J. Kauwe, A. C. in Thought Study Investigators *et al.*, “Religious orders study/memory and aging project investigators; alzheimer’s disease genetics consortium,” *Genetically predicted body mass index and Alzheimer’s disease-related phenotypes in three large samples: Mendelian randomization analyses*. *Alzheimers Dement*, vol. 11, no. 12, pp. 1439–1451, 2015.
- [49] D. A. Bennett, J. A. Schneider, Z. Arvanitakis, and R. S. Wilson, “Overview and findings from the religious orders study,” *Current Alzheimer Research*, vol. 9, no. 6, pp. 628–645, 2012.
- [50] P. De Jager, Y. Ma, C. McCabe, J. Xu, B. Vardarajan, D. Felsky, H. Klein, C. White, M. Peters, B. Lodgson *et al.*, “A multi-omic atlas of the human frontal cortex for aging and alzheimer’s disease research. sci data 5: 180142,” 2018.
- [51] C. Wah, S. Branson, P. Welinder, P. Perona, and S. Belongie, “The caltech-ucsd birds-200-2011 dataset,” 2011.
- [52] X. Wang, D. Kumar, N. Thome, M. Cord, and F. Precioso, “Recipe recognition with large multimodal food dataset,” in *2015 IEEE International Conference on Multimedia & Expo Workshops (ICMEW)*. IEEE, 2015, pp. 1–6.